Supplementary Information

The enzyme-like catalytic activity of CeO2 nanoparticles and its dependency on Ce^{3+} surface area concentration

V. Baldim*, F. Bedioui, N. Mignet, I. Margaill and J.-F. Berret*

Outline

Supporting Information S1 – Transmission Electronic Microscopy (TEM) micrographs

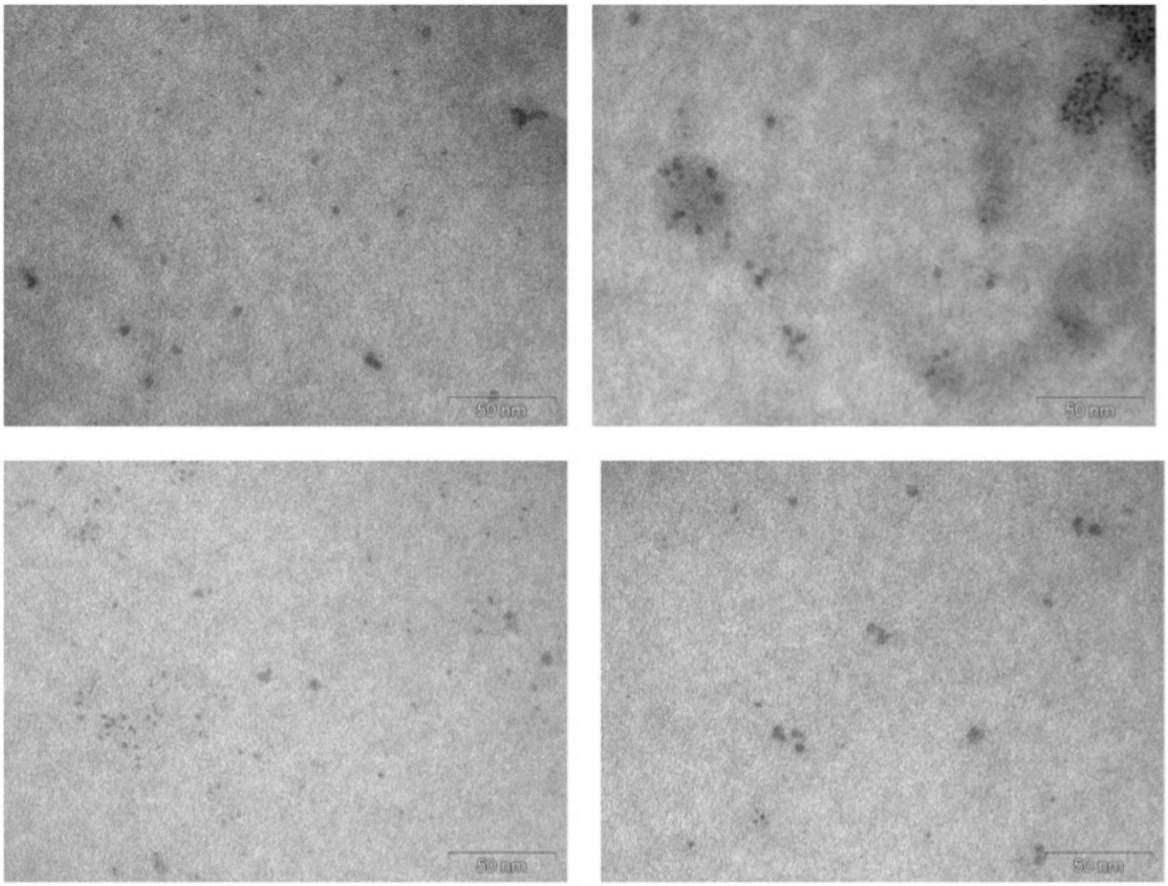

Figure S1a: TEM micrographs of CNP-5.

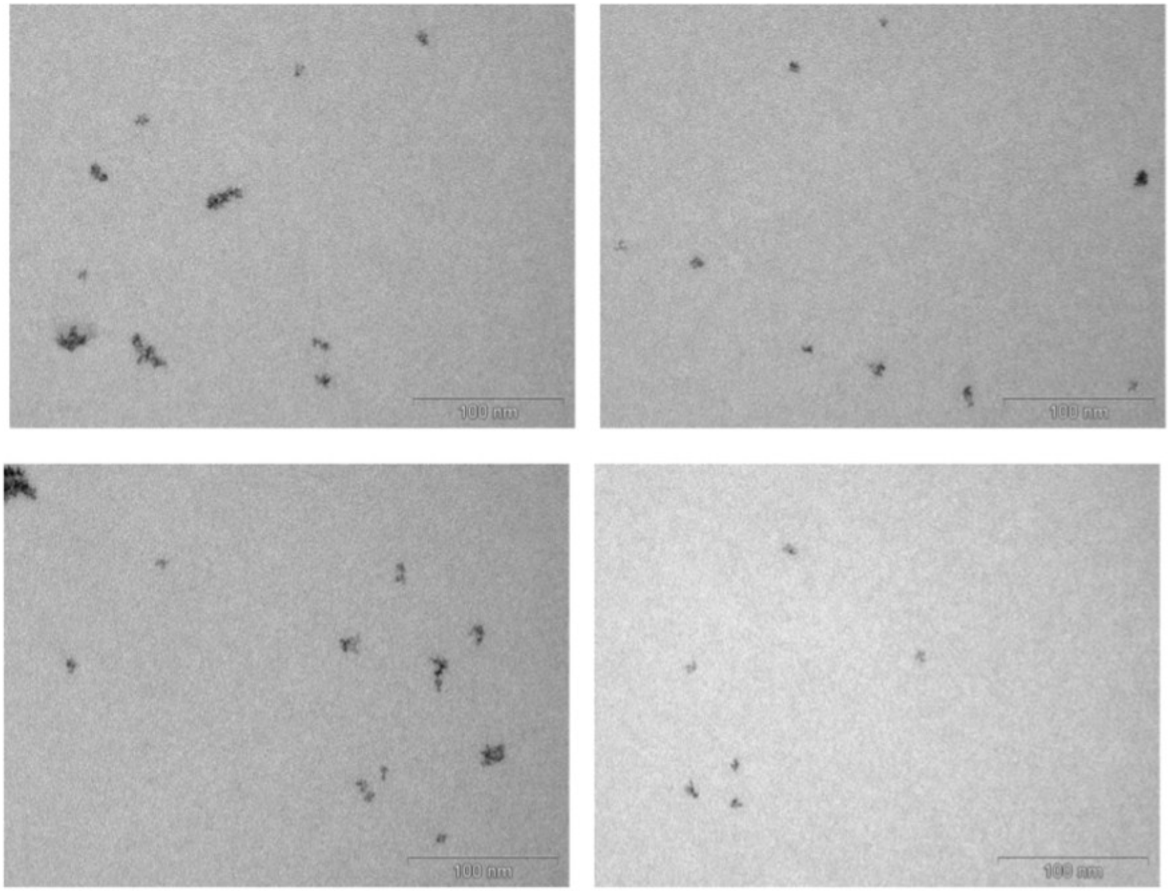

Figure S1b: TEM micrographs of CNP-8. The particles are similar to those shown by TEM or cryo-TEM in refs. [1-4]

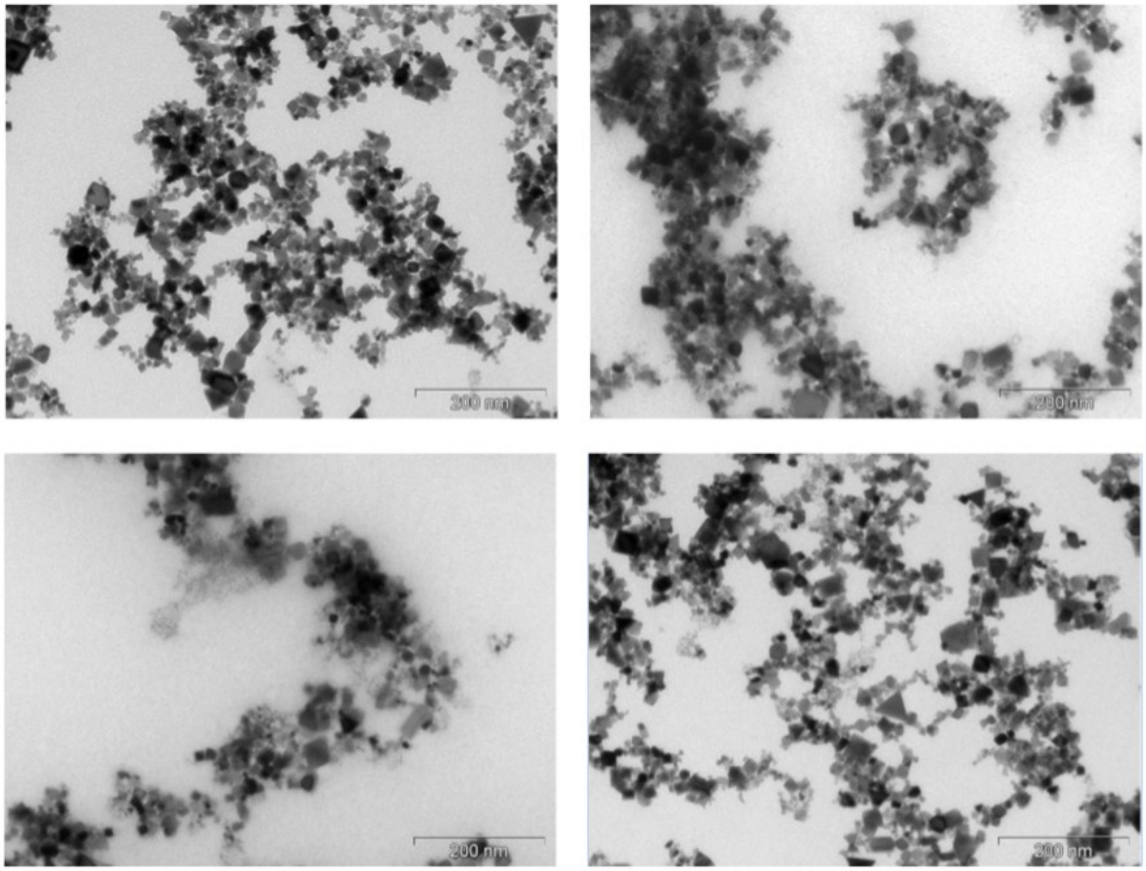

Figure S1c: TEM micrographs of CNP-23.

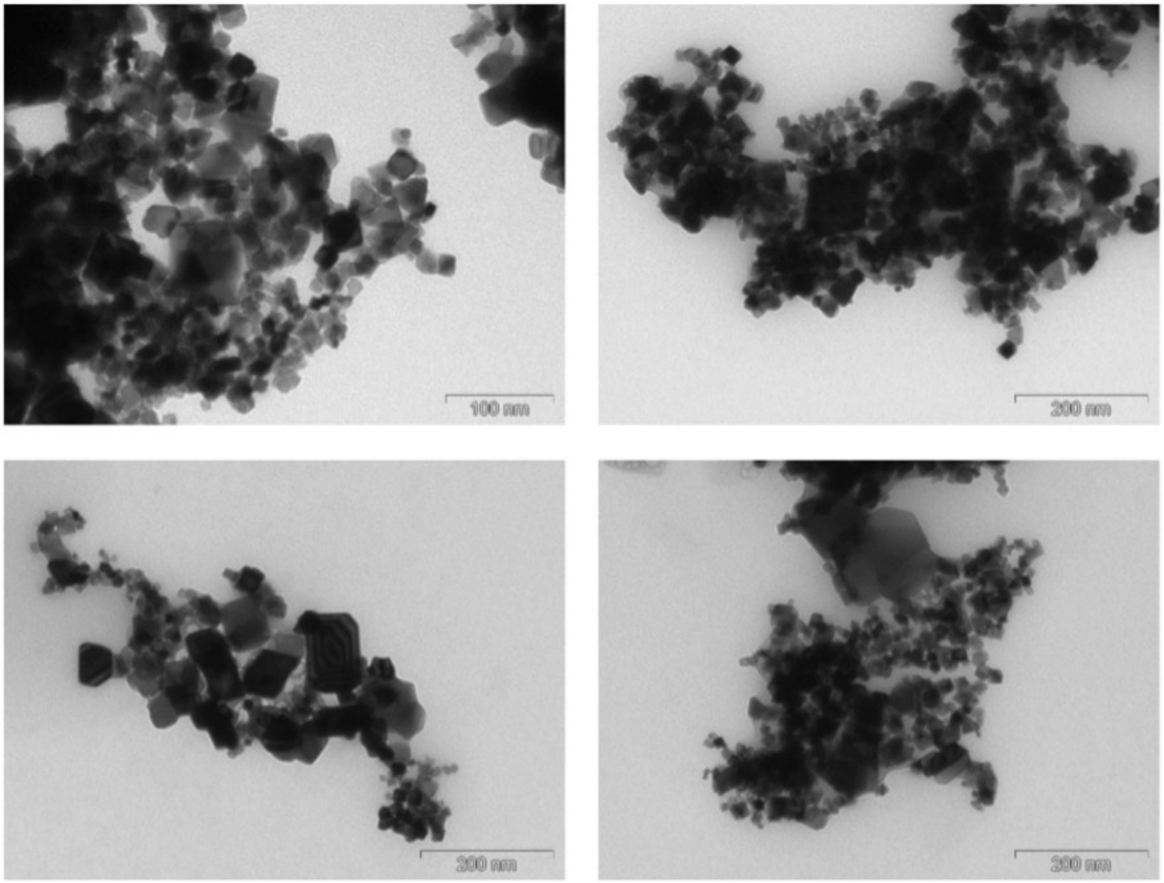

Figure S1d - TEM micrographs of CNP-28. CNP-28 is a benchmark material (code name NM-212) synthesized for the Organisation for Economic Co-operation and Development (OECD) program "*Testing a representative set of manufactured nanomaterials*".[5]

Supporting Information S2 – List and definitions of parameters used in the manuscript

Parameter	unit	Definition
Particle characteristics		
D	nm	Nanoparticle median diameter
s		Size dispersity
ρ	g cm^{-3}	Particle density
$M_n^{CeO_2}$	g mol^{-1}	Number-averaged molecular weight of CeO_2 nanoparticle
$M_w^{CeO_2}$	g mol^{-1}	Weight-averaged molecular weight of CeO_2 nanoparticle
Concentration		
[Ce]	M	Cerium molar concentration
c	g L^{-1}	Cerium oxide weight concentration
$f_{Ce^{3+}}$	%	Ce^{3+} fraction
A_S	m^2 g^{-1}	Specific surface area
c_S	m^2 L^{-1}	Surface area concentration
$c_S f_{Ce^{3+}}$	m^2 L^{-1}	Ce^{3+} surface area concentration
A_{ES}	g^{-1} m^2	Effective specific surface
c_{ES}	m^2 L^{-1}	Effective surface area concentration
$c_{ES} f_{Ce^{3+}}$	m^2 L^{-1}	Ce^{3+} effective surface area concentration
Catalytic activity		
A_{SOD}	%	Superoxide radical dismutation
A_{CAT}	%	Hydrogen peroxide disproportionation

Nanoparticle median diameter D and dispersity s

The median particle diameter D and the dispersity s are derived from the TEM size distributions shown in Fig. 1. The distributions are fitted using a log-normal function of the form:

$$p(d,D,s) = \frac{1}{\sqrt{2\pi}\beta(s)d} exp\left(-\frac{ln^2(d/D)}{2\beta(s)^2}\right) \qquad (S2.1)$$

In the previous equation, $\beta(s)$ is related to the size dispersity s by the relationship $\beta(s) = \sqrt{ln(1+s^2)}$. s is defined as the ratio between the standard deviation and the average diameter [6]. For β < 0.4, one has $\beta \cong s$ [3,4,7].

Number- and weight averaged molecular weight of CeO_2 nanoparticle: $M_n^{CeO_2}$ and $M_w^{CeO_2}$

The number-average molecular weight $M_n^{CeO_2}$ writes:

$$M_n^{CeO_2} = \frac{\pi}{6}\rho D^3 exp(4.5s^2)N_A \qquad (S2.2)$$

For log-normal distribution of median diameter D and dispersity s, the ith-moment is given by the expression $< D^i > = D_0^i exp(i^2 s^2/2)$. In Eq. S2.2, ρ = 7.1 g cm^{-3} is the mass density and N_A the Avogadro number [8].

Along the same line, the weight-average molecular weight $M_w^{CeO_2}$ writes [9]:

$$M_w^{CeO_2} = \frac{\pi}{6}\rho D^3 exp(13.5s^2)N_A \qquad (S2.3)$$

The molar-mass dispersity $Đ(s)$ for the particles then writes [8,9]:

$$Đ(s) = \frac{M_w^{CeO_2}}{M_n^{CeO_2}} = exp(9s^2) \qquad (S2.4)$$

As expected, uniform colloids are characterized by $s = 0$ and $Đ = 1$.

Ce^{3+} fraction $f_{Ce^{3+}}$
The Ce^{3+} fraction is estimated from X-ray photoelectron spectrometry (XPS) as:

$$f_{Ce^{3+}} = \frac{Ce^{3+}}{Ce^{3+} + Ce^{4+}} \qquad (S2.5)$$

where Ce^{3+} and Ce^{4+} are determined from the fitting of the Ce 3d spectra integrated intensities (see S3).

Specific surface area A_S
The specific surface area A_S is defined as the ratio between the particle surface and its mass. Taking into account the dispersity, one gets:

$$A_S = \frac{\pi D^2 exp(2s^2)}{\rho(\pi/6)D^3 exp(4.5s^2)} = 6\exp(-2.5s^2)/\rho D \qquad (S2.6)$$

Surface area concentration c_S and $c_S f_{Ce^{3+}}$

The surface area concentration is the product of the actual weight concentration c (in g L^{-1}) and the specific surface area A_S (in m^2 g^{-1}):

$$c_S = \frac{6c\exp\left(-2.5s^2\right)}{\rho D} = A_S\, c \qquad (S2.7)$$

c_S is then expressed in m^2 L^{-1}. The product $c_S f_{Ce^{3+}}$ then represents the Ce^{3+} surface area concentration.

Effective Specific surface area A_{ES} and Surface area concentration c_{ES}

The effective parameters c_{ES} and $c_{ES} f_{Ce^{3+}}$ are determined using the effective specific surface area A_{ES} which is calculated from A_S (Eq. S2.6) and from a normalizing coefficient measured from amperometry (Table 2)

Catalytic activity A_{SOD} and A_{CAT}

The SOD and CAT catalytic activities of nanoceria A_{SOD} and A_{CAT} are defined as the percentages of dismutated superoxide radicals and of decomposed H_2O_2 respectively, as determined at the end of the assay.

Supporting Information S3 – X-ray photoelectron spectrometry (XPS) Ce 3d spectra

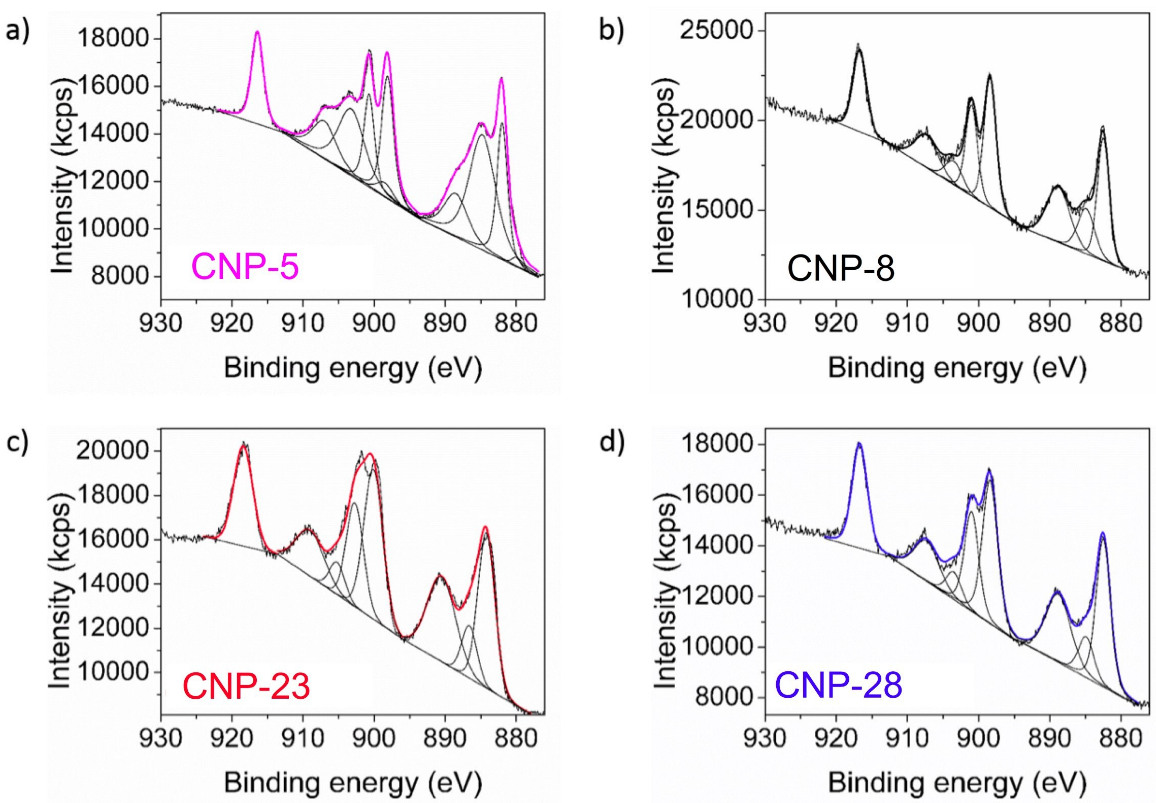

Figure S3 - Decomposed XPS spectra for the Ce 3d core level in nanoceria. The peaks are due to ejected Ce3d electrons from Ce^{4+} and Ce^{3+} whose states and binding energies are detailed in Table S1. There are 3 peaks associated with Ce^{4+} ions and 2 peaks associated with Ce^{3+} ions each of them split in two, $Ce3d_{5/2}$ (V^i) and $Ce3d_{3/2}$ (U^i) states, presenting a constant separation of ~18.5 eV. The three doublets corresponding to Ce^{4+} are U''' (916.7 eV)/V''' (898.4 eV), U (901.0 eV)/V (882.5 eV), U'' (907.3 eV)/V'' (888.8 eV) and the two doublets corresponding to Ce^{3+} are U' (903.5 eV)/V' (884.9 eV), U_o (898.8 eV)/V_o (880.3 eV)).[5] The spectra were decomposed using the free software XPSPEAKS 4.1. Some conditions were assumed for spectrum deconvolution: 1) Gaussian-Lorentzian curves were used for the individual peaks, the weight of the Gaussian Lorentzian contribution being optimized for the U''' peak and fixed for all the others; 2) the full width at half maximum (FWHM) of split peaks have the same values. The fraction of Ce^{3+} ions was calculated from the integrated intensities of the XPS peaks through Eq. S2.

$$Ce^{3+} = \frac{U' + V' + Uo + Vo}{U''' + V''' + U + V + U'' + V'' + U' + V' + Uo + Vo} 100\% \qquad \text{Equation S2}$$

Table S3 – Parameters and integrated intensities of peaks from XPS Ce 3d spectra of nanoceria and the Ce^{3+} fraction calculated.

Ion	State	Binding energy (eV)	CNP-5	CNP-8	CNP-23	CNP-28
Ce^{4+}	U'''	916.7	9794/1.96/43	11933/2.13/13	15432/3.15/3	12427/2.53/24
	V'''	898.4	12999/1.96/43	16579/2.13/13	23149/3.15/3	16984/2.53/24
	U	901.0	8844/1.75/43	11375/1.95/13	14411/2.85/3	11086/2.38/24
	V	882.5	12974/1.75/43	15391/1.95/13	21616/2.85/3	16485/2.38/24
	U''	907.3	8099/3.96/43	7860/3.83/13	10397/4.69/3	7765/4.1/24
	V''	888.8	9310/3.96/43	13397/3.83/13	19471/4.89/3	13142/4.1/24
Ce^{3+}	U'	903.5	15823/4.37/43	4213/2.75/13	3969/2.51/3	3251/2.54/24
	V'	884.9	27141/4.37/43	7991/2.75/13	6445/2.51/3	4876/2.54/24
	U_o	898.8	2093/2.71/43	0/-/-	0/-/-	0/-/-
	V_o	880.3	736/2.71/43	0/-/-	0/-/-	0/-/-
Ce^{3+} (%)			**42.5**	**13.8**	**9.06**	**9.45**

[a] FWHM stands for Full width at half maximum; [b] Gaussian/Lorentzian percentage on fitted curves

Supporting Information S4 – Wide-Angle X-Ray Scattering (SAXS)

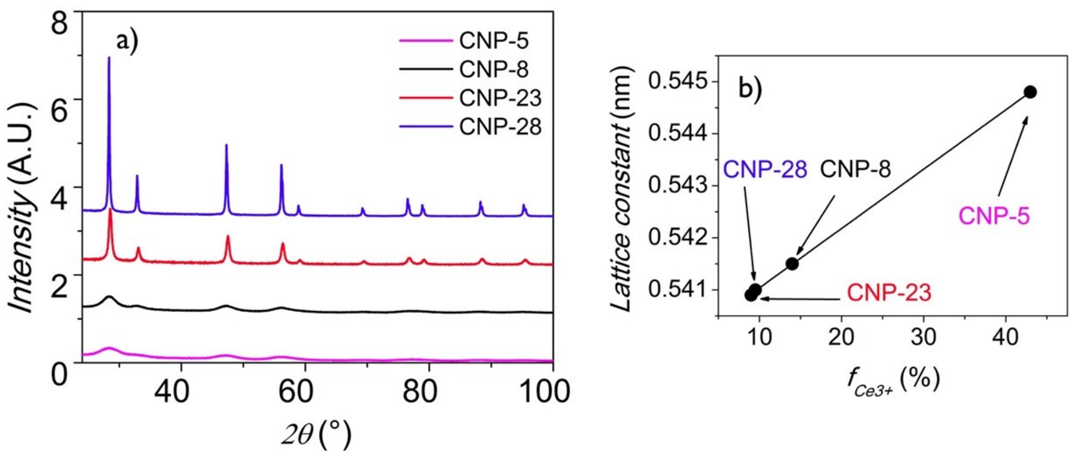

c)

CeO_{2-x} nanoparticles	D_{TEM} (nm)	dispersity	crystallite size (nm)	lattice constant (nm)
CNP-5	4.5	0.36	1.9	0.544572
CNP-8	7.8	0.17	3.3	0.541514
CNP-23	23	0.42	16.4	0.540858
CNP-28	28	0.31	43.3	0.540999

Figure S4: a) Diffractogram of CNP-5, CNP-8, CNP-23 and CNP-28 obtained by WAXS. The positions of the Bragg peaks index for fluorite structure, space group Fm3m. b) Nanoceria lattice constants obtained by Rietveld Maud method as a function of the Ce^{3+} fraction obtained by XPS. The lattice constant increases linearly with the Ce^{3+} fraction, in agreement with Vegard's law [10]. c) Particle characteristics obtained from TEM and WAXS.

Supporting Information S5 – UV-vis absorption spectra

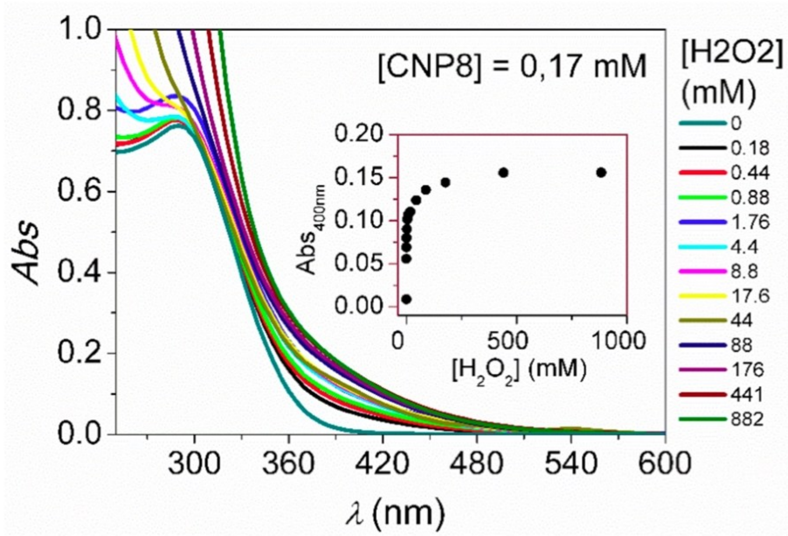

Figure S5a: UV-vis spectra of a dispersion of CNP-8 ([Ce] = 0.17 mM) after addition of hydrogen peroxide to final concentrations varying from 0 to 882 mM. Inset: Absorption at 400 nm in function of the final hydrogen peroxide concentration.

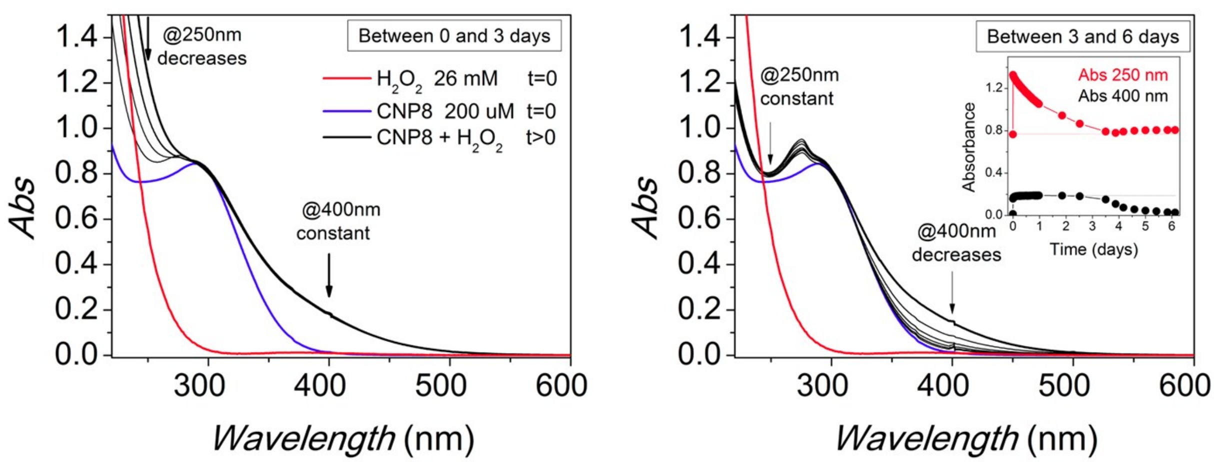

Figure S5b: UV-vis spectra of a dispersion of CNP-8 as a function of the wavelength at different times after the addition of H2O2. Left-hand side: between 0 and 3 days; Right-hand side: between 3 and 6 days. Inset: UV-Vis adsorption kinetics at 250 and 400 nm. In these figures, it can be seen that the spectra return to their initial state, confirming the catalytic cycling properties of nanoceria.

Supporting Information S6 – Superoxide dismutase (SOD)-like activity

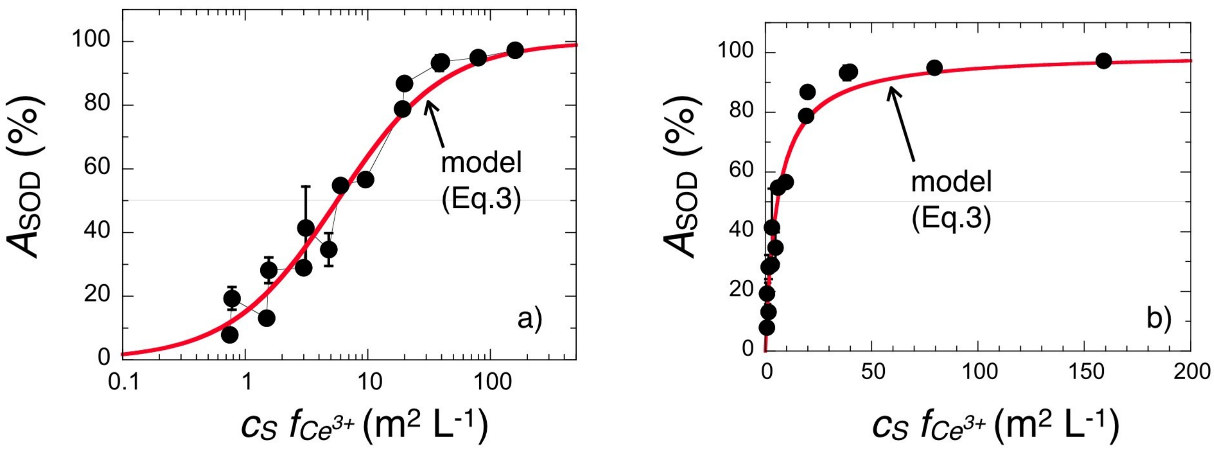

Figure S6: Fitting the SOD-like activity data as function of the effective surface area concentration *times* the Ce^{3+} percentage. The data in a) are in semi-log scales whereas those in b) and in linear scales.

Supporting Information S7 – Catalase (CAT)-like activity

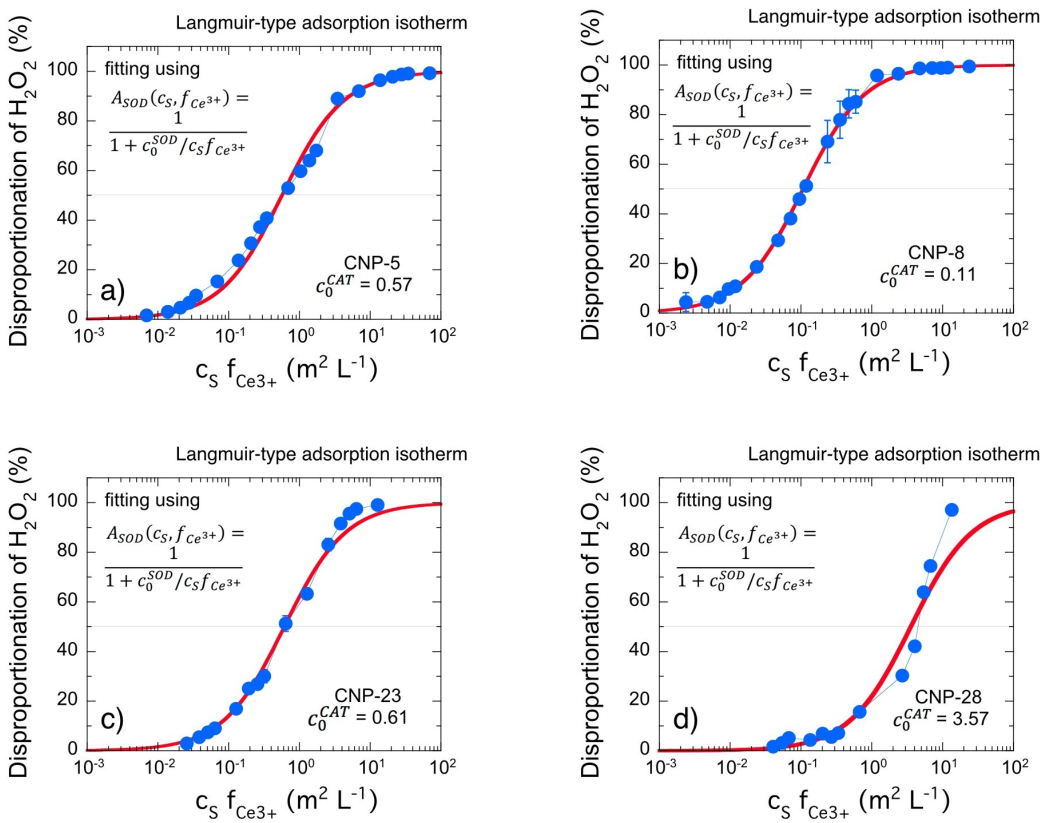

Figure S7a: Fitting the CAT-like activity data as function of the effective surface area concentration *times* the Ce3+ percentage for the four CNPs: a) CNP-5; b) CNP-8; c) CNP-23 and d) CNP-28.

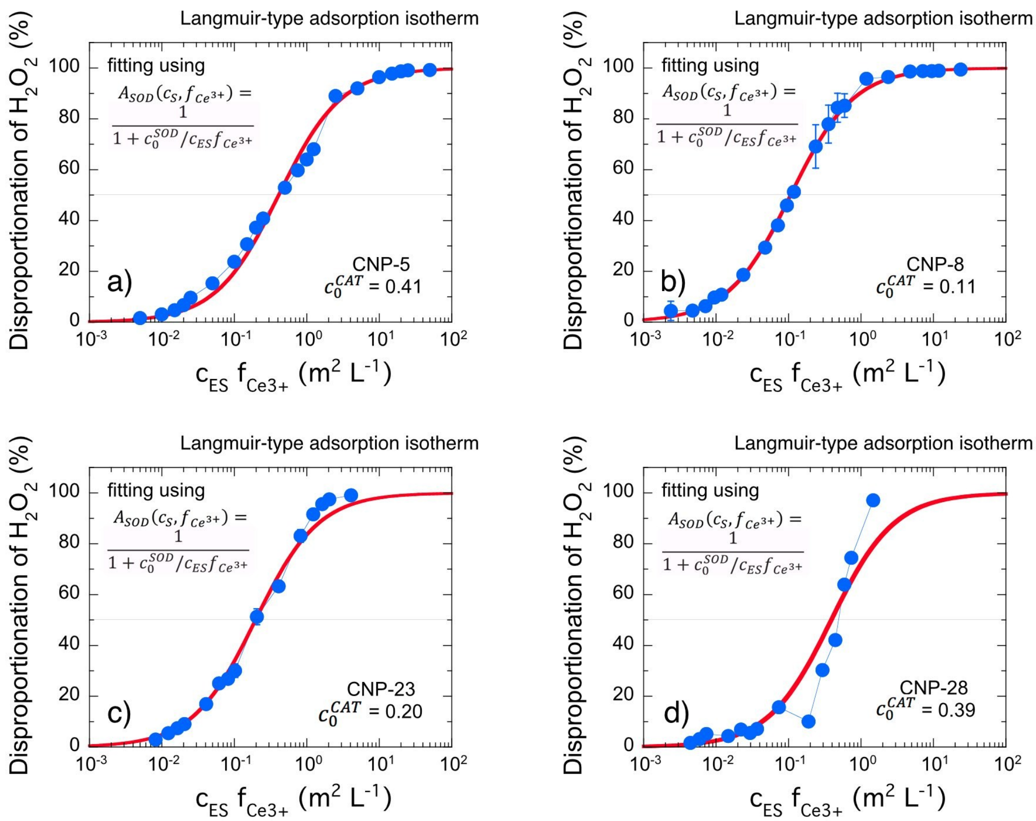

Figure S7b: Same as in Fig. 7a using the effective surface area concentration *times* the Ce^{3+} percentage.

References

[1] J.-F. Berret, A. Sehgal, M. Morvan, et al., Stable oxide nanoparticle clusters obtained by complexation, *J. Colloid Interface Sci.*, **303** (2006) 315-318.
[2] L. Qi, J.P. Chapel, J.C. Castaing, et al., Organic versus hybrid coacervate complexes: co-assembly and adsorption properties, *Soft Matter*, **4** (2008) 577-585.
[3] L. Qi, A. Sehgal, J.C. Castaing, et al., Redispersible hybrid nanopowders: Cerium oxide nanoparticle complexes with phosphonated-PEG oligomers, *ACS Nano*, **2** (2008) 879-888.
[4] A. Sehgal, Y. Lalatonne, J.-F. Berret, et al., Precipitation-redispersion of cerium oxide nanoparticles with poly(acrylic acid): Toward stable dispersions, *Langmuir*, **21** (2005) 9359-9364.
[5] C. Singh, S. Friedrichs, G. Ceccone, et al., Cerium Dioxide, NM-211, NM-212, NM-213. Characterisation and test item preparation, European Commission Joint Research Centre Institute for Health and Consumer Protection, Ispra, Italy, 2014.

[6] R. Klein, B. D'aguanno, Static Scattering Properties of Colloidal Suspensions, in: W. Brown (Ed.) Light Scattering, Principles and Developments, Oxford, 1996, pp. 30 - 102.
[7] J.-F. Berret, O. Sandre, A. Mauger, Size distribution of superparamagnetic particles determined by magnetic sedimentation, *Langmuir*, **23** (2007) 2993-2999.
[8] F. Mousseau, L. Vitorazi, L. Herrmann, et al., Polyelectrolyte assisted charge titration spectrometry: Applications to latex and oxide nanoparticles, *J. Colloid Interface Sci.*, **475** (2016) 36-45.
[9] V. Torrisi, A. Graillot, L. Vitorazi, et al., Preventing Corona Effects: Multiphosphonic Acid Poly(ethylene glycol) Copolymers for Stable Stealth Iron Oxide Nanoparticles, *Biomacromolecules*, **15** (2014) 3171-3179.
[10] S. Tsunekawa, K. Ishikawa, Z.Q. Li, et al., Origin of anomalous lattice expansion in oxide nanoparticles, *Phys. Rev. Lett.*, **85** (2000) 3440-3443.